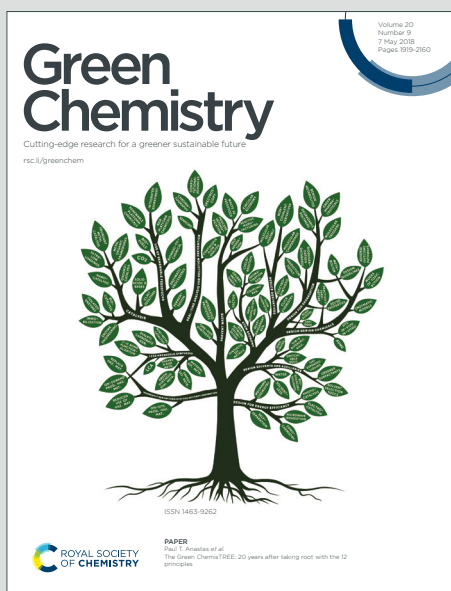


Green Chemistry

Cutting-edge research for a greener sustainable future

Accepted Manuscript

This article can be cited before page numbers have been issued, to do this please use: X. Wang, Y. Yang, H. Zhong, T. Wang, J. Cheng and F. Jin, *Green Chem.*, 2020, DOI: 10.1039/D0GC02785E.



This is an Accepted Manuscript, which has been through the Royal Society of Chemistry peer review process and has been accepted for publication.

Accepted Manuscripts are published online shortly after acceptance, before technical editing, formatting and proof reading. Using this free service, authors can make their results available to the community, in citable form, before we publish the edited article. We will replace this Accepted Manuscript with the edited and formatted Advance Article as soon as it is available.

You can find more information about Accepted Manuscripts in the [Information for Authors](#).

Please note that technical editing may introduce minor changes to the text and/or graphics, which may alter content. The journal's standard [Terms & Conditions](#) and the [Ethical guidelines](#) still apply. In no event shall the Royal Society of Chemistry be held responsible for any errors or omissions in this Accepted Manuscript or any consequences arising from the use of any information it contains.

Molecular H₂O promoted catalytic bicarbonate reduction with methanol into formate over Pd_{0.5}Cu_{0.5}/C under mild hydrothermal conditions

Received 00th January 20xx,
Accepted 00th January 20xx

DOI: 10.1039/x0xx00000x

www.rsc.org/

Xiaoguang Wang,^a Yang Yang,^a Heng Zhong,^{*a,b,c} Tianfu Wang,^{a,c} Jiong Cheng,^a and Fangming Jin^{*a,b,c}

Direct reduction of bicarbonate, a typical product of CO₂ captured in alkaline solution, into value-added organics is one promising way to achieve a simplified and green CO₂ capture and utilization process. In this work, a new strategy of bicarbonate reduction coupled with methanol oxidation to a dual formation of formate at mild hydrothermal conditions is reported. A 68% formate production efficiency based on the reductant methanol and nearly 100% selectivity of formate were obtained via a Pd_{0.5}Cu_{0.5}/C catalyst at 180 °C. An *operando* hydrothermal ATR-FTIR study proved that the bicarbonate was reduced by the *in situ* generated hydrogen from methanol, which was stepwise oxidized to formaldehyde and formic acid. Notably, DFT calculation and qNMR study of ¹³C and ²H (D) isotopic labelling revealed that H₂O molecules not only supplied the hydrogen for bicarbonate reduction but also acted as an indispensable promoter to enhance the catalytic performance of Pd_{0.5}Cu_{0.5}/C for methanol activation.

1. Introduction

Reduction of CO₂, a typical greenhouse gas, to useful chemicals has shown considerable environmental and economic benefits since the fixation of CO₂ would significantly alleviate the associated environmental risks and the stress of fossil fuel depletion. Although the direct conversion of CO₂ – from industrial flue gas have been reported,¹ CO₂ is generally needed to be captured from either atmosphere or point sources by commonly using alkaline absorbents before further utilization. This process transforms the CO₂ into HCO₃⁻ and/or CO₃²⁻ (the final products are pH-dependent).^{2,3} However, as shown in Fig. 1, the current technologies for CO₂ conversion are mainly limited in gaseous CO₂ transformation.⁴⁻⁶ Thus, the captured CO₂ (in the form of HCO₃⁻ and/or CO₃²⁻) needs to be regenerated and released at a relatively high dissociation temperature of *ca.* 200 – 1000 °C and re-compressed to high-pressure CO₂ gas before being applied with these methods, which is not only complicated but also consumes huge energies.⁷ On the other hand, HCO₃⁻ is the dominant substance (nearly 100%) among all the dissolved carbon species (CO₂(aq),

H₂CO₃, HCO₃⁻, CO₃²⁻) in a CO₂ saturated alkaline solution.⁸ If the captured CO₂ could be converted directly in the form of HCO₃⁻, not only much energy will be saved but also the process of CO₂ capture and utilization will be greatly simplified. Therefore, the direct reduction of HCO₃⁻ could be considered as a promising greener strategy for CO₂ capture and utilization.

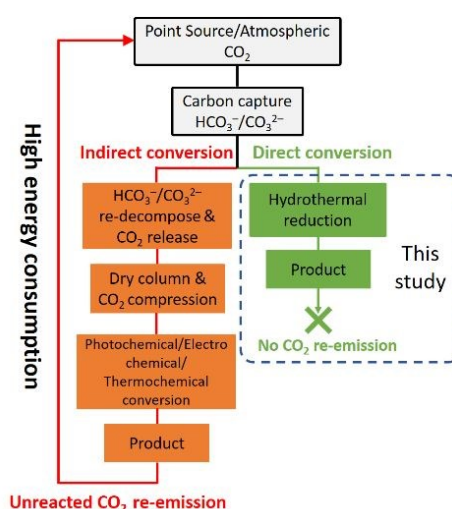


Fig. 1 Scheme of CO₂ capture and utilization – a comparison of previous methods and this study.

Among the organics derived from CO₂/HCO₃⁻, formic acid is one of the most important products due to its versatile application in modern chemical industry. More importantly,

^a School of Environmental Science and Engineering, State Key Lab of Metal Matrix Composites, Shanghai Jiao Tong University, Shanghai 200240, China

^b Center of Hydrogen Science, Shanghai Jiao Tong University, Shanghai, 200240, China

^c Shanghai Institute of Pollution Control and Ecological Security, Shanghai 200092, P.R. China

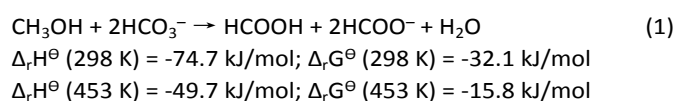
* Fangming Jin: fmjin@sjtu.edu.cn; Heng Zhong: zhong.h@sjtu.edu.cn.

† Electronic supplementary information (ESI) available. See DOI: 10.1039/x0xx00000x

formic acid with a 4.4 wt.% hydrogen content has been recently regarded as a promising hydrogen carrier because of its stability, low toxicity, biodegradability, and convenience in storage and transportation.^{9, 10} Current methods of formic acid production generally require fossil-based CO and extensive alkali, suffering from environmental threat and heavy reliance on fossil feedstock. Thus, replacing CO with HCO₃⁻ for the formic acid production, especially when driven by renewable energy, could be an ideal green and clean strategy for formic acid generation.

For the CO₂/HCO₃⁻ reduction, high-pressure H₂ gas is usually an indispensable element, which is currently mainly derived from non-renewable natural gas and petroleum,^{11, 12} resulting in energy consumption and environmental problems. In addition, the use of high-pressure H₂ gas involves energy consumption, storage, and transportation issues. On the other hand, biomass or their derivatives rich in reducing functional groups show great potential to offer renewable alternatives for molecular H₂, which can act as active hydrogen donors through the pathway known as aqueous reforming with the assistance of hydrothermal reactions.^{13, 14} Meanwhile, hydrothermal environment has been verified to show robustness for HCO₃⁻ reduction according to our previous works.^{15, 16} Thus, with the *in situ* generated hydrogen from biomass hydrothermal reforming, HCO₃⁻ reduction is expected to be achieved in a H₂-free pathway under hydrothermal conditions.^{17, 18}

Methanol (CH₃OH) has a wide application in chemical reaction, and can be easily produced from renewable sources such as biomass.¹⁹ It has been reported that over 300,000 metric tons of methanol was annually produced from renewable resource in the United States.²⁰ Given to the functional group of -OH stored in methanol, it can be served as one clean, efficient and renewable hydrogen source, which makes it a highly potential hydrogen source for HCO₃⁻ reduction. More importantly, as shown in eqn (1), HCO₃⁻ reduction with methanol can achieve a dual formation of formic acid/formate simultaneously, indicating good energy efficiency and high atomic economy can be obtained.



While the overall reduction of HCO₃⁻ with methanol into formate is thermodynamically favourable, a reasonable catalyst is expected to drive the reaction more efficient. Pd-based materials are well-known hydrogenation catalysts due to their excellent hydrogen absorption capacity,^{21, 22} however, the high cost and limited reserve impeded its wide application. Diluting Pd with earth-abundant materials is a feasible and facile strategy to decrease the cost of Pd-based catalysts and to further increase its catalytic performance and stability.^{23, 24} Cu is one of the most extensively studied metal catalysts for CO₂ hydrogenation.²⁵ Also, Cu has been reported to be efficient in activating alcohols due to the enrichment of atomic oxygen species at copper surface and sub-/near-surface region to form a copper suboxide phase during the reaction, which can

effectively bind and activate the alcohol molecules.^{26, 27} Therefore, combining metallic Pd catalyst with Cu would probably be a logical strategy to catalyse the HCO₃⁻ reduction with methanol effectively.

In general, heterogeneous catalysts are the primary target for development due to their prominent role in catalysing the reaction. However, since the catalysis occurs at interfacial sites, substances in liquid or gaseous phases can also affect the catalytic properties.²⁸ In a typical hydrothermal reaction, water is generally considered to be an environmentally benign medium due to its unique inherent properties of high ion product (K_w) and low dielectric constant under high temperature and high pressure.²⁹ However, beyond the well-known function as solvent, there is evidence that the water was indispensable for the hydrothermal conversion of biomass and HCO₃⁻ based on previous works,^{30, 31} but the mechanism is still unknown.

Here, we propose a new route of HCO₃⁻ reduction into formate with methanol as the reductant under mild hydrothermal conditions. Methanol was oxidized into formate simultaneously, which led to a dual formation of formate. Results showed that HCO₃⁻ could be reduced efficiently at 180 °C on a Pd_{0.5}Cu_{0.5}/C catalyst. More importantly, H₂O was found to not only serve as an environmental-benign solvent but also act as a bridge for methanol activation and oxidation to produce H₂ and thereby achieve the HCO₃⁻ reduction. Also, loads of effort are paid in this research on exploring the role of H₂O with the aid of ¹³C- and ²H-qNMR and DFT study. The presented study proposed a new and green method of direct reduction of bicarbonate with alcohols as renewable hydrogen sources to achieve a dual formation of formic acid/formate in one-step. These results could provide new insights in developing a simplified and greener process for CO₂ capture and utilization.

2. Experimental

2.1 Materials

Methanol (CH₃OH, 99.9%), palladium chloride (PdCl₂, 99.99%) and copper nitrate trihydrate (Cu(NO₃)₂·3H₂O, 99.99%) were purchased from Shanghai Macklin Biochemical Technology Co., Ltd. Sodium bicarbonate (NaHCO₃, 99.9%) was purchased from Sinopharm Chemical Reagent Co., Ltd and was selected as the CO₂ source for considerations that NaHCO₃ is the main product of trapping CO₂ from waste streams by alkaline solutions. Cabot Vulcan XC-72 carbon was used as the catalyst support. D₂O (99.9%, Sinopharm Chemical Reagent Co.), NaH¹³CO₃ (99%, Sigma-Aldrich), H¹³C₂COOH (≥95%, J Cambridge Isotope Laboratories Ltd.) and CH₃¹³C₂COOH (≥95%, J Cambridge Isotope Laboratories Ltd.) were used for determination of formate source. All reagents were used without further purification. Deionized water was used throughout the study.

2.2 Catalyst Preparation

Pd_{0.5}Cu_{0.5}/C catalyst with a 7.5 wt.% total loading was prepared by an impregnation method. First, a certain amount of PdCl₂ was dissolved into 1 mol/L HCl to obtain a 0.2 mol/L H₂PdCl₄

solution. Then, 1.05 mL of 0.2 mol/L H_2PdCl_4 and 5 mL 11.4 g/L $\text{Cu}(\text{NO}_3)_2 \cdot 3\text{H}_2\text{O}$ solution were slowly added into a 100 mL flask and mixed with 0.4625 g carbon powder under vigorously stirring. The pH of the mixture was increased to 10 by adding 0.5 mol/L NaOH solution. After stirring for 24 hours, 10 mL of 2 mol/L NaBH_4 was added dropwise into the mixture. After continuous stirring for another 12 hours, the black suspension was filtered, washed with deionized water thoroughly and dried in a vacuum dryer to obtain the final $\text{Pd}_{0.5}\text{Cu}_{0.5}/\text{C}$ catalyst. By keeping the total loading of metals (Pd and Cu) at 7.5 wt.%, Pd-Cu catalysts with different molar ratios ($\text{Pd}_{0.75}\text{Cu}_{0.25}/\text{C}$, $\text{Pd}_{0.66}\text{Cu}_{0.33}/\text{C}$, $\text{Pd}_{0.33}\text{Cu}_{0.66}/\text{C}$ and $\text{Pd}_{0.25}\text{Cu}_{0.75}/\text{C}$) as well as Pd/C and Cu/C were also prepared by using similar method, and the ICP-OES results of each catalysts were summarized in Table S1 †.

2.3 Experimental procedures

In this study, all experiments were conducted in a stainless-steel (SUS 316) tubular reactor (3/8 inch o.d., 1-mm wall thickness) with an inner volume of 5.7 mL. The schematic drawing of the reacting system can be found in our previous research.³² A typical reaction procedure was as follow: 0.1 mol/L methanol, 1 mol/L NaHCO_3 and 50 mg catalyst were loaded into the reactor. Then, the reactor was sealed and put into a salt bath which was preheated to a desired temperature. After a certain reaction time, the reactor was removed out of the salt bath and quickly submerged into a cold-water bath to quench the reaction. The liquid and solid samples were separated through a 0.22 μm syringe filter and collected for further analysis. Gas sample was collected by a water-gas replacement method in a measuring cylinder immersed in a saturated NaCl aqueous solution tank.

In this study, the amount of formate obtained from the HCO_3^- by one hydroxyl is used to evaluate the efficiency of NaHCO_3 reduction with methanol (abbreviated as 'formate production efficiency'). The detailed definition can be found in ESI †.

2.4 Analytical methods

Liquid samples were analysed by high-performance liquid chromatography (HPLC), gas chromatography-mass spectrometry (GC-MS), gas chromatography-flame ionization detector (GC-FID) and $^{13}\text{C}/^2\text{H}$ -quantitative nuclear magnetic resonance ($^{13}\text{C}/^2\text{H}$ -qNMR). Gas samples were characterized by GC-MS and quantified by gas chromatography-thermal conductivity detector (GC-TCD). Solid samples were analysed by X-ray diffractometer (XRD), X-ray photoelectron spectroscopy (XPS) and transmission electron microscope (TEM). *Operando* hydrothermal ATR-FTIR was employed to monitor the reaction process (Fig. S1 †). The detailed analytical conditions can be found in ESI †.

3. Results and discussion

3.1 Characterization of catalysts

First, the $\text{Pd}_{0.5}\text{Cu}_{0.5}/\text{C}$ catalyst was prepared and characterized. For comparison, a Pd/C catalyst was also synthesized by the similar procedure without adding the Cu precursor. SEM image

showed that nanoparticles (NPs) of ca. 100 nm were observed for the $\text{Pd}_{0.5}\text{Cu}_{0.5}/\text{C}$ catalyst, which should be associated to the carbon support since similar morphologies were also observed for Pd/C and carbon black particle samples (Fig. S2 and S3 †). TEM image of the $\text{Pd}_{0.5}\text{Cu}_{0.5}/\text{C}$ catalyst showed that metal nanoparticles with an average diameter of 3.4 ± 0.3 nm was successfully dispersed on the carbon support (Fig. 2a). Composition of the NPs was verified by an energy-dispersive X-ray spectroscopy (EDS) analysis, which clearly demonstrates that Cu and Pd atoms are randomly and homogeneously distributed in each NPs (Fig. 2b-e), suggesting PdCu alloy was successfully formed. In a high-resolution TEM (HRTEM) image of a typical NP from $\text{Pd}_{0.5}\text{Cu}_{0.5}/\text{C}$ (Fig. 2f), the measured lattice distance was 2.28 Å, which can be attributed to the 1/3(422) fringes of PdCu alloy face-centred cubic structure.³³⁻³⁵ In addition, the Pd nanoparticles had an average diameter of 2.6 nm from the TEM image of Pd/C (Fig. S4 †). From the XRD patterns (Fig. 2g), both Pd/C and $\text{Pd}_{0.5}\text{Cu}_{0.5}/\text{C}$ showed a broad

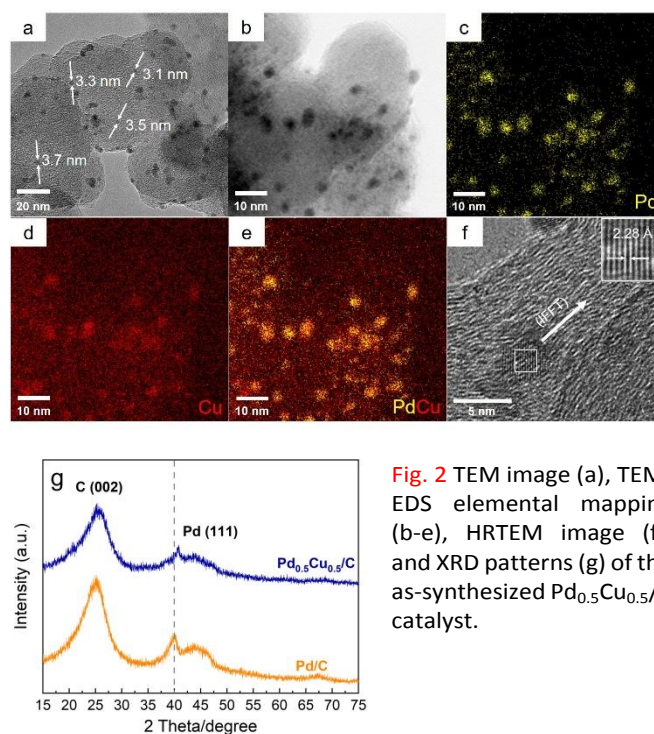


Fig. 2 TEM image (a), TEM-EDS elemental mapping (b-e), HRTEM image (f), and XRD patterns (g) of the as-synthesized $\text{Pd}_{0.5}\text{Cu}_{0.5}/\text{C}$ catalyst.

peak located at around 25° , which was attributed to the (002) plane of carbon with hexagonal structure. The diffraction pattern of Pd/C showed a weak peak located at around 40° , which is attributed to the (111) plane of the Pd face-centred cubic (fcc) structure (ICDD 46-1043). On the other hand, Pd alloying with Cu caused the diffraction peaks of Pd in the $\text{Pd}_{0.5}\text{Cu}_{0.5}/\text{C}$ catalyst to shift slightly to higher 2θ values. ICP-OES analysis of the $\text{Pd}_{0.5}\text{Cu}_{0.5}/\text{C}$ revealed that the weight percentage of Pd and Cu were 4.46% and 2.68%, respectively, which were close the designed values (Pd 4.5 wt.% and Cu 3.0 wt.%). In brief, a carbon-supported PdCu alloy NP catalyst was successfully synthesized.

3.2 HCO₃⁻ reduction with methanol over Pd_{0.5}Cu_{0.5}/C catalyst

Possibility of HCO₃⁻ reduction with methanol as the reductant and Pd_{0.5}Cu_{0.5}/C as the catalyst was investigated. Results showed that formate were successfully produced after the reaction as predicted, and the total formate concentration was 121.9 mmol/L. For comparison, formic acid production from methanol alone was investigated in the absence of NaHCO₃ (Table 1). However, only negligible trace amount of formic acid was produced when CH₃OH reacted alone. Furthermore, even 1 mol/L NaOH was added to adjust the reaction pH, only 21.1 mol/L formate was produced without the addition of NaHCO₃, which was much lower than that (121.9 mmol/L) obtained with NaHCO₃. These results indicated the participation of NaHCO₃ in the formation of formate. It should be noted that the formate and formic acid displayed a single peak in the HPLC analysis (Fig. S5†). Since both formic acid and formate were produced from the reaction of methanol with HCO₃⁻ (eqn (1)), ¹³C-qNMR measurement was performed to distinguish and quantify the NaHCO₃-sourced formate and CH₃OH-sourced formic acid. In a labelling experiment using NaH¹³CO₃ (Fig. S6†), a strong signal associated with H¹³COO⁻ was observed at 171.2 ppm. The concentration of NaH¹³CO₃-sourced formate was determined to be 67.3 mmol/L by adding 50 mmol/L CH₃¹³COOH as an internal standard. Based on the NaHCO₃-sourced formate concentration determined by qNMR and the total formate concentration determined by HPLC, a quantification of NaHCO₃-sourced formate and CH₃OH-sourced formic acid was summarized in Table 1. Results revealed that the NaHCO₃-sourced formate and CH₃OH-sourced formic acid were 67.3 and 54.6 mmol/L, respectively, which indicates a dual formation of formate/formic acid from NaHCO₃ and CH₃OH was achieved. In addition, formaldehyde (HCHO) was also detected by GC-MS, suggesting that CH₃OH was stepwise oxidized into formaldehyde and formic acid. It is encouraging that the selectivity of formate was nearly 100% although a trace amount of HCHO was detected in liquid samples. GC-TCD analysis for gaseous samples was further applied and only H₂ was observed (Table 1). These results indicate that the coexistence of NaHCO₃ and CH₃OH is beneficial necessary to the formation of formate.

Table 1 Product distribution of NaHCO₃ reduction with methanol^a

	Liquid products (mmol/L)		Gaseous products (mL)	
	NaHCO ₃ sourced	CH ₃ OH sourced	HCHO	H ₂
with NaHCO ₃	67.3	54.6	Trace	10.1 ml
w/o NaHCO ₃	-	Trace	-	Trace
w/o NaHCO ₃ ^b	-	21.1	Trace	13.5 ml

^a Reaction condition: 0.1 mol/L CH₃OH, 1 mol/L NaHCO₃, 50% water filling, 50 mg Pd_{0.5}Cu_{0.5}/C, 180 °C, and 16 h. ^b 1 mol/L NaOH was added to simulate the alkalinity induced by NaHCO₃.

3.3 Reaction characteristics and catalyst stability

View Article Online

DOI: 10.1039/D0GC02785E

To enhance the production of formate from the NaHCO₃ reduction with methanol, effects of different reaction parameters such as reaction temperature, time (Fig. S7†) and catalyst amount (Fig. S8†) were investigated. The temperature profile shows that only a trace amount of formate was formed at 150 °C. Increasing the temperature significantly promoted the formation of formate, especially when the temperature exceeded 160 °C. On the other hand, when temperature reached 180 °C, the formate production efficiency increased continuously with the extension of time. However, the reaction tended to slow down when the reaction time exceeded 16 h. At 200 °C, a high efficiency of 75% from NaHCO₃ was obtained. The effect of catalyst amount results showed that increasing the catalyst amount lead to an obvious promotion in the production of formate. However, when the catalyst amount reached 50 mg, further increase in catalyst amount had no significant effect on the reaction efficiency. Stability of the Pd_{0.5}Cu_{0.5}/C catalyst was further examined. Although a slight decrease in the formate production efficiency was observed in the 2nd cycle, further decline was not observed in the following 5 cycles (Fig. S9†). The Pd_{0.5}Cu_{0.5}/C catalyst after reaction was collected and analysed by SEM, TEM and XRD (Fig. S10†). Results showed that the morphology and crystallinity of Pd_{0.5}Cu_{0.5}/C catalyst had no obvious change after the reaction. However, TEM analysis revealed that the PdCu alloy slightly aggregated after the reaction, and the NPs size increased to ca. 4.5 nm, which probably caused the decrease in formate production efficiency in the 2nd cycle. ICP analysis of the liquid sample after the reaction discovered no dissolved Pd or Cu species. These results indicated that the Pd_{0.5}Cu_{0.5}/C catalyst was relatively stable.

3.4 Catalytic property and mechanism

Based on the detected intermediates of HCHO and H₂ (Table 1), the overall process of CH₃OH reacting with NaHCO₃ could be divided into two parts: the hydrogen generation from methanol oxidation, which contains two steps (eqn (2) and (3)), and the HCO₃⁻ hydrogenation to formate (eqn (4)).



Then, the catalytic property of Pd_{0.5}Cu_{0.5}/C for these two parts were studied separately to explore the catalytic mechanism. First, H₂ production from methanol oxidation was investigated in the presence and absence of Pd_{0.5}Cu_{0.5}/C catalyst. For comparison, results obtained from Pd/C, Cu/C catalyst were also employed. As summarized in Table 2, only trace amount of H₂ was produced in the absence of any catalyst and in the presence of carbon black (Table 2, Entries 1 and 2). On the other hand, H₂ generation was clearly promoted when Pd/C, Pd_{0.5}Cu_{0.5}/C and Cu/C were used, and the Pd_{0.5}Cu_{0.5}/C catalyst exhibited the best performance (Table 2, Entries 3-5). The TON for hydrogen generation obtained on Pd_{0.5}Cu_{0.5}/C was 1.4 and 3.8 times higher than those obtained on Pd/C and Cu/C,

respectively. These results indicate that Pd_{0.5}Cu_{0.5}/C could effectively promote methanol hydrothermal reforming for hydrogen generation. Subsequently, NaHCO₃ hydrogenation with *ex situ* gaseous H₂ on the Pd_{0.5}Cu_{0.5}/C, Pd/C, and Cu/C were studied. Results showed that no formate production was observed in the absence of any catalyst, and a significant formate increase appeared in the presence of Pd_{0.5}Cu_{0.5}/C catalyst (Table S2 †). The above results demonstrated that Pd_{0.5}Cu_{0.5}/C catalyst played irreplaceable part in both H₂ generation from methanol and NaHCO₃ hydrogenation.

In addition, the effect of different Pd/Cu ratio (molar ratio) on hydrogen generation and formate production were tested (Table 2, Entries 4, and 6-9). Pd_{0.5}Cu_{0.5}/C exhibited the highest catalytic activities in formate production, indicating that a 1:1 Pd/Cu ratio was the optimum condition (Table 2, Entry 4). Notably, it was less sensitive for formate production when the molar ratio of Pd was higher than 50% (Table 2, Entries 6 and 7). On the other hand, increasing the proportion of Cu could improve the efficiency of H₂ generation, however, excessive Cu was unfavourable for the formate production. Therefore, Pd is the core component in the PdCu alloy catalyst, and the introduction of Cu not only effectively reduced the cost of precious metal, but also improved the hydrogen generation and further formate production.

Table 2 Hydrogen generation and formate production efficiency obtained from different catalysts^a

Entry	Catalyst	TON of hydrogen generation ^b (mol H ₂ per mol PdCu)	Formate production efficiency (%) ^c
1	None	Trace	Trace
2	carbon black	Trace	Trace
3	Pd/C	10.4	46.3
4	Pd _{0.5} Cu _{0.5} /C	14.3	67.6
5	Cu/C	3.8	15.2
6	Pd _{0.75} Cu _{0.25} /C	12.8	67.0
7	Pd _{0.66} Cu _{0.33} /C	13.1	67.5
8	Pd _{0.33} Cu _{0.66} /C	9.0	38.1
9	Pd _{0.25} Cu _{0.75} /C	7.6	22.2
10 ^d	Pd _{0.5} Cu _{0.5} /C	Trace	Trace

^a H₂ generation and formate production are two independent experiments. ^b Reaction condition: 0.1 mol/L CH₃OH, 1 mol/L NaOH, 50% water filling, 50 mg catalysts, 180 °C, and 16 h. ^c Reaction condition: 0.1 mol/L CH₃OH, 1 mol/L NaHCO₃, 50% water filling, 50 mg catalysts, 180 °C, and 16 h. ^d Methanol was used as a solvent instead of water, and other conditions are the same as "b" and "c".

The interaction between Pd and Cu should have an indispensable role in hydrogen generation and NaHCO₃ hydrogenation. To further verify the property of PdCu alloy, XPS analysis was conducted. Fig. 3 illustrates the XPS results of Pd_{0.5}Cu_{0.5}/C and Pd/C before reaction. Compared to Pd/C, the Pd 3d peaks of PdCu alloy shifted to a lower binding energy. For Pd/C, the Pd 3d_{5/2} and Pd 3d_{3/2} peaks centred at 335.9 and 341.3 eV, respectively, while for Pd_{0.5}Cu_{0.5}/C, the position of Pd 3d_{5/2}

and Pd 3d_{3/2} peaks shifted to 335.3 and 340.6 eV, respectively. This is probably attributed to a smaller electron negativity of Cu than that of Pd, which leads to an electron injection from Cu to Pd.^{36, 37} The XPS result of Cu can be found in Fig. S11 †. These results indicated that the incorporation of Cu could change the electronic structure of Pd, further leading to a downward shift of Pd d-band centre.³⁸ The shift of d-band centre resulted in a decrease in the binding energy of hydrogen on Pd surface, which positively improved the catalytic performance of Pd for hydrogen generation.^{39, 40} On the other hand, when compared to the unalloyed state, the electronic structure of Pd modified by Cu doping caused Pd d-band centre to be far away from its Fermi level.^{38, 41} The farther d-band centre of transition metals to their Fermi level, the lower adsorption energy on transition metal surface for C1 products.^{42, 43} Thus, the formate adsorption enthalpy on the PdCu alloy surface became lower than that on the single Pd. As a result, when formate was formed on PdCu alloy, it detached from the catalyst surface, leading to an enhanced formate production and selectivity of formate from HCO₃⁻ reduction. In brief, Pd should be the core reaction site for both steps of hydrogen generation and formate production, while the introduction of Cu improved Pd performance by altering the electronic structure of Pd.

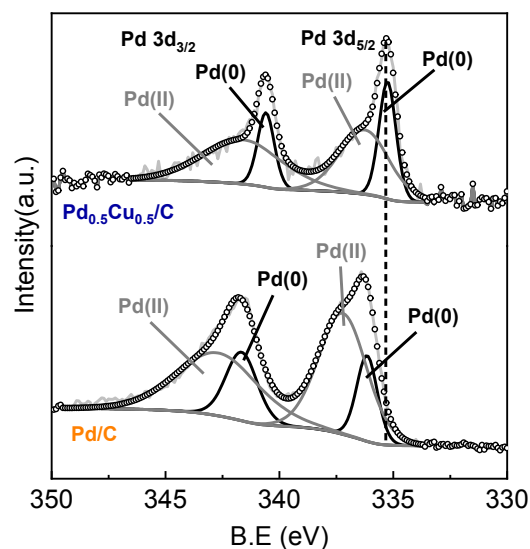


Fig. 3 XPS spectra of Pd 3d in Pd_{0.5}Cu_{0.5}/C and Pd/C.

3.5 Role of H₂O

As shown in eqn (3), one obvious role of H₂O was to react with HCHO to produce H₂, indicating that H₂O participated in the reaction as a hydrogen source. However, H₂ and HCHO was hardly detected when methanol reacting with HCO₃⁻ in the absence of H₂O (Table 2, Entry 10), indicating that H₂O was also indispensable for the first step of methanol activation (eqn (2)). To further verify the role of H₂O and its mechanism, DFT calculations were performed on the process of hydrogen generation from methanol with or without H₂O. The structures of methanol molecule, transition state without H₂O, and the transition state with H₂O were determined, which are shown in

Fig. 4a, b and c, respectively. The transition state structure exhibited a narrow angle of 1C-5O-6H in the absence of H₂O (Fig. 4b), which was significantly bent (from 108.9 ° to 53.6 °) as compared with that of the equilibrium structure of the isolated methanol (Fig. 4a). This result indicates that the H₂ generation from methanol without H₂O requires overcoming a huge potential energy barrier. On the other hand, the 1C-5O-6H angle

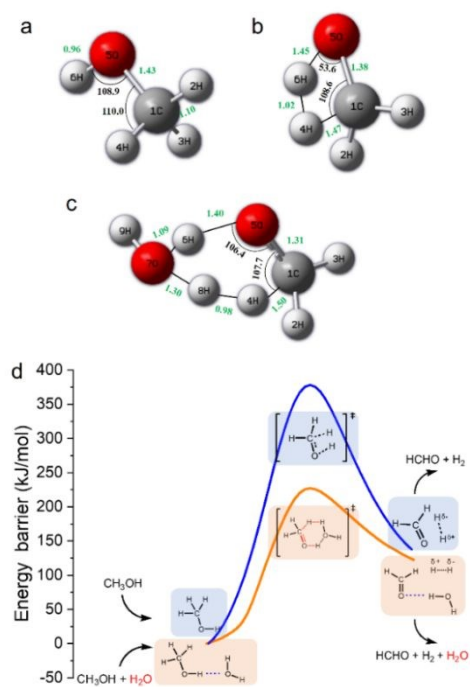
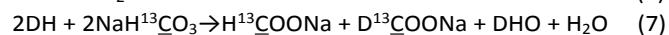


Fig. 4 Transition states (a)-(c) and energy profiles (d) for methanol dissociation into H₂ with or without H₂O (a: methanol molecule; b: the transition state without H₂O; c: the transition state with H₂O; d: the profile with H₂O as the promoter is depicted in orange while the profile without H₂O is depicted in blue).

relaxed to 106.4 ° in the presence of H₂O (Fig. 4c), which is nearly comparable to that of the isolated methanol. Moreover, the added H₂O molecule (7O-8H-9H) behaves as a proton acceptor and formed a deformed H₃O-cation-like conformation with the transition state atom 6H from methanol molecule, which would drastically reduce the activation energy for the ionic water dissociation. As a result of these effects, the energy barrier of hydrogen generation from methanol with H₂O addition was significantly reduced (from 378 kJ/mol to 220 kJ/mol) compared to that in the absence of H₂O (Fig. 4d), suggesting the critical role of H₂O as a promoter in this process. Then, the corresponding reaction mechanism based on the calculation results is proposed in Fig. 4d. One H₂O molecule acts as a bridge for methanol breaking down to produce one H₂ and one HCHO. Thus, it is suggested that the H₂ generated from methanol in eqn (2) should consist of one atom from methanol and one atom from H₂O. Based on these results, eqn (2-4) could be re-written as isotope-labelled forms (eqn (5-7)) for a better

understanding the mechanism, in which D₂O and NaH¹³CO₃ were used instead of H₂O and NaHCO₃, respectively. This leads to the NaH¹³CO₃-sourced formate consisted of H¹³COO⁻ and D¹³COO⁻ in the ratio of 1:1.



To further confirm the DFT calculation results and above assumption (eqn (5-7)), isotopic tracing reaction with D₂O substituting of H₂O was conducted. In the meantime, NaH¹³CO₃ was used instead of NaHCO₃ to trace the reaction path of carbon. It should be noted first that we confirmed that the H of -CH₃ in CH₃OH, -CH in HCHO or HCOO⁻ would not undergo hydrogen-deuterium exchange under hydrothermal conditions in an independent run (Fig. S12[†]). As displayed in Fig. 5a, the peak assigned to D¹³COO⁻ was clearly observed in the D-qNMR spectrum, and it consisted of 2 parallel peaks, while the corresponding ¹³C-qNMR image showed that NaH¹³CO₃ sourced formate contained 3 parallel peaks, which was caused by the resonance effect between ¹³C and D (Fig. 5a, b). The COSY spectra of the liquid sample after NaH¹³CO₃ reacting with methanol in D₂O was also shown in Fig. 5c. These results confirmed that formate from NaHCO₃ reduction carried D from D₂O. Furthermore, the concentration of D-labelled and ¹³C-labelled formate were determined with dimethyl sulfoxide-D₆ and CH₃¹³COOH as the internal standards, respectively.⁴⁴ The results showed the final product of formate was comprised of nearly identical amount of H¹³COO⁻ and D¹³COO⁻ (Table 3), which was perfectly consistent with the DFT calculations and further confirmed the promoting effect of H₂O in methanol activation.

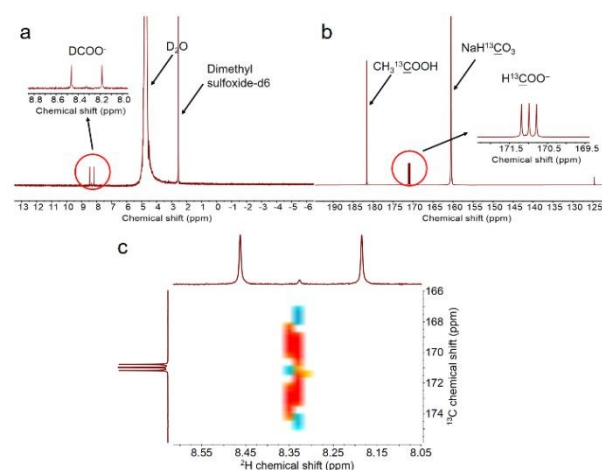


Fig. 5 D-qNMR (a), ¹³C-qNMR (b) and COSY spectra (c) of the liquid sample after NaH¹³CO₃ reacting with methanol in D₂O (reaction conditions: 0.1 mol/L CH₃OH, 1 mol/L NaH¹³CO₃, 50% D₂O filling, 50 mg Pd_{0.5}Cu_{0.5}/C, 180 °C, and 16 h; dimethyl sulfoxide-D₆ and CH₃¹³COOH were used as the internal standards to calculate D-labelled and ¹³C-labelled formate concentration, respectively).

Table 3 Product distribution of NaH¹³CO₃ reduction with methanol in D₂O^a

Formate concentration (mmol/L)	NaH ¹³ CO ₃ sourced		CH ₃ OH sourced	Total
	H ¹³ COO ⁻	D ¹³ COOH ⁻		
	33.3	32.1	53.1	118.5

^a Reaction conditions: 0.1 mol/L CH₃OH, 1 mol/L NaH¹³CO₃, 50% D₂O filling, 50 mg Pd_{0.5}Cu_{0.5}/C, 180 °C, and 16 h.

In summary, the results of DFT and ¹³C/²H-qNMR clearly demonstrated that H₂O played as a promoter for methanol activation in eqn (2). Thus, the total three roles of H₂O in the process of HCO₃⁻ reduction with methanol can be summarized as: (1) acting as an indispensable promoter by lowering the reaction energy barrier of methanol activation into formaldehyde; (2) reacting with formaldehyde to release hydrogen; (3) serving as a green solvent.

It should be noted that according to eqn (1), the ratio of CH₃OH-sourced HCOOH to the HCO₃⁻-sourced HCOO⁻ should be 1:2. However, our isotopic results showed that the actual ratio of CH₃OH-sourced HCOOH to the HCO₃⁻-sourced HCOO⁻ was ca. 1:1.2. These results suggested that in the reduction of HCO₃⁻ with CH₃OH, the first part (eqn (2) and (3)) was easier to react than the second part (eqn (4)). Thus, unreacted H₂ product was detected in the gaseous phase.

3.6 Operando ATR-FTIR study

To obtain a full understanding of the reaction mechanism, an *operando* hydrothermal ATR-FTIR was further carried out to examine the transformation of reactants. All the *operando* ATR-FTIR spectra were collected as subtraction spectrum with the initial state (25 °C, before starting the heating reaction) as background. First, the spectrum during the reaction with or without catalyst were captured. As shown in Fig. 6a, the peaks at 1633 cm⁻¹ and 1400 cm⁻¹ are assigned to the asymmetrically and symmetrically adsorbed HCO₃⁻ (COO bond), respectively.^{45, 46} The 1012 cm⁻¹ peaks can be ascribed to the C-O bond of adsorbed CH₃OH, and the vibration signals caused by metal-O bond at 840 cm⁻¹ and 713 cm⁻¹ also confirmed the adsorption of methanol on the catalyst surface.⁴⁷ Furthermore, the vibration peak due to the adsorption of reactants tended to weaken as the reaction proceeds, indicating that the HCO₃⁻ and CH₃OH were consumed for further reaction on the Pd_{0.5}Cu_{0.5}/C surface.

Then, as shown in Fig. 6b, upon heating the mixture of CH₃OH and NaHCO₃ in aqueous solution, peaks located at 1585 cm⁻¹ and 1385 cm⁻¹, which represented the OCO asymmetric and symmetric stretches of HCOO⁻, appeared and intensified gradually with increasing temperature, and the peak of C-H bond stretching vibration at 2850 cm⁻¹ related to HCOO⁻ also increased gradually. These results indicate that formate production rate was promoted with temperature and time increasing. The main formaldehyde bands are located at 2923, 2853, and 1354 cm⁻¹ based on the previous report,⁴⁸ however, the peaks at 2923 and 2853 cm⁻¹ overlapped with formate ν(C-H) bands in Fig. 6b, indicating that they were difficult to distinguish. On the other hand, the band at 1354 cm⁻¹,

belonging to the ω(C-H) of formaldehyde, was clearly observed at 100 °C and its absorbance signal increased with the reaction temperature. Nevertheless, when temperature reached 180 °C, the formaldehyde vibration disappeared with prolonged time, this was probably attributed to rapid transformation of formaldehyde to formate during the reaction, making it difficult to capture. Furthermore, the peaks at 1110 and 1082 cm⁻¹, which could be assigned to the C-O bond of methanol, was blue-shifted along with the increase in reaction time. This was probably attributed to the methanol oxidation into formaldehyde, that is the transforming from C-O bond to C=O bond, causing the increase in bonding energy of C-O bond.

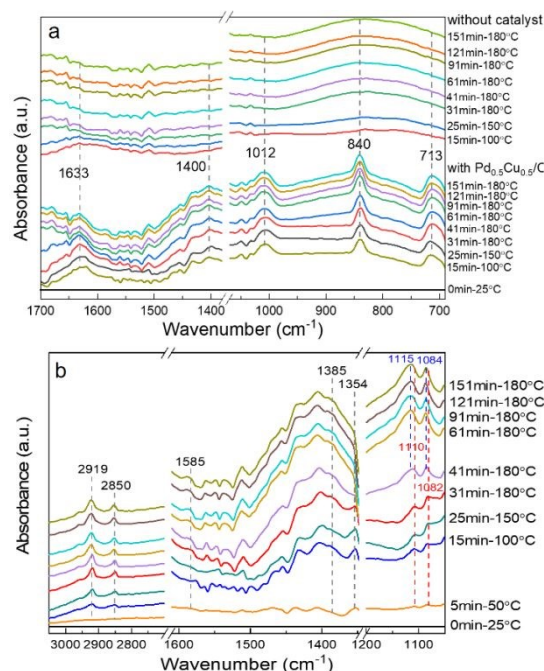


Fig. 6 *Operando* ATR-FTIR subtraction spectra recorded during HCO₃⁻ reduction with methanol (All the spectra subtracted the spectrum of the initial state as the background; initial state: 0.1 mol/L CH₃OH, 1 mol/L NaHCO₃, 100% water filling, 5 mg Pd_{0.5}Cu_{0.5}/C, 25 °C; (a) ATR-FTIR spectra comparison with or without catalyst; (b) temperature and time sequence spectra of *operando* ATR-FTIR obtained with Pd_{0.5}Cu_{0.5}/C catalyst; test condition: 0.1 mol/L CH₃OH, 1 mol/L NaHCO₃, 100% water filling, 5 mg Pd_{0.5}Cu_{0.5}/C).

3.7 Reaction mechanism

Based on the above research, a possible reaction mechanism of HCO₃⁻ reaction with methanol in water on Pd_{0.5}Cu_{0.5}/C is proposed in Fig. 7. First, CH₃OH (i) is oxidized into HCHO (iii) on the catalyst with a H₂ generation through the promotion effect of H₂O molecule. Then, the formed HCHO (iii) reacts with a second H₂O molecule to produce another H₂ and HCOOH (v). Thus, one CH₃OH molecule produces two molecules of H₂ with one H₂O molecule as the promoter and another as the hydrogen source. Subsequently, the formed *in situ* H₂ and HCO₃⁻ are activated by adsorbing on the Pd_{0.5}Cu_{0.5}/C surface ((vii) and

(viii)), and then the activated H nucleophilic attacks the C=O, leading to the formation of HCOO⁻ ((ix) and (x)) through the cleavage of C-OH bond.

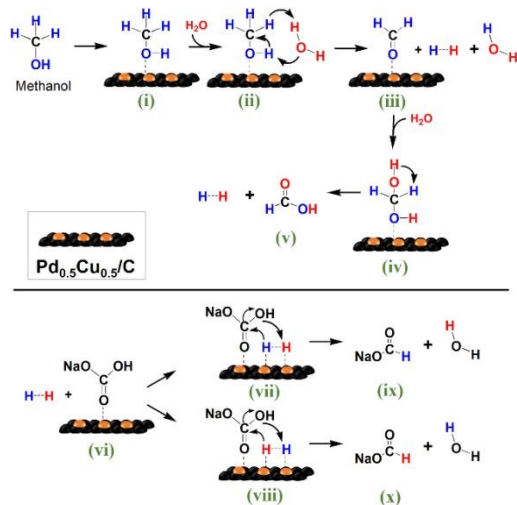


Fig. 7 Reaction scheme of HCO₃⁻ reduction into formate with methanol in water on Pd_{0.5}Cu_{0.5}/C catalyst.

3.8 Universality research

Applicability of the hydrothermal reduction of various inorganic carbon sources with different alcohols were examined. As summarized in Table 4, when gaseous CO₂ was used as the starting material instead of bicarbonate, only trace amount of formate was detected (Table 4, Entry 2), suggesting CO₂ gas was hardly to be directly converted in this system. However, when 1 mol/L NaOH was added, a 48.6% formate production efficiency was successfully obtained (Table 4, Entry 3), which should be attributed to the transformation of CO₂ to HCO₃⁻ in NaOH solution. This result further suggests that a one-step CO₂ capture and conversion reaction can be achieved by using the presented method. Furthermore, other carbonates and bicarbonates such as K₂CO₃, KHCO₃, and Na₂CO₃ were also tested, and the formate production efficiency reached 87.3%, 70.5% and 83.4%, respectively (Table 4, Entries 4-6). Notably, the hydrogenation of carbonates is generally more difficult than that of bicarbonates because the protonation of carbonate ions was considered to be inferior in aqueous solutions.^{49, 50} To our delight, the carbonates showed better performance than the corresponding bicarbonates in the presented research. This is probably due to the weak acidity of methanol was enhanced by the hydrothermal reaction, which then attacked the inert CO₃²⁻ and made it more reactive than the *ex situ* HCO₃⁻.

In addition, the activity of various alcohols using as reductant for the hydrothermal reduction of HCO₃⁻ was examined. Results revealed that ethanol, 1-propanol and 1-butanol exhibited similar activity to methanol in the reduction of HCO₃⁻ to formate, while themselves were converted to corresponding acids (Table 4, Entries 8-10, Fig. S13[†]). Notably, the reactivity of alcohols slightly increased with the growth of the carbon chains and the 1-butanol exhibited the best activity for HCO₃⁻

reduction. Based on the above results, the alcohol bicarbonate system can be expected to be applied to the synergistic conversion of various hydroxyl-rich organics and CO₂ sources.

Table 4 Reduction of various CO₂ sources with different alcohols^a

Entry	Alcohols	Carbon source ^b	Formate production efficiency (%)
1	methanol	-	Trace
2	methanol	CO ₂	Trace
3 ^c	methanol	CO ₂	48.6
4	methanol	K ₂ CO ₃	87.3
5	methanol	KHCO ₃	70.5
6	methanol	Na ₂ CO ₃	83.4
7	methanol	NaHCO ₃	67.6
8	ethanol	NaHCO ₃	68.9
9	1-propanol	NaHCO ₃	72.3
10	1-butanol	NaHCO ₃	73.4

^a Reaction condition: 0.1 mol/L alcohol, 1 mol/L HCO₃⁻ or CO₃²⁻, 50% water filling, 50 mg Pd_{0.5}Cu_{0.5}/C, 180 °C, and 16 h.

^b CO₂: 2.5 MPa, others: 1 mol/L. ^c 1 mol/L NaOH was added.

4. Conclusions

In summary, we have developed an efficient strategy for HCO₃⁻ reduction with methanol as hydrogen source on a Pd_{0.5}Cu_{0.5}/C catalyst under mild hydrothermal conditions. A 68% formate production efficiency and nearly 100% selectivity of formate from bicarbonate were obtained via a Pd_{0.5}Cu_{0.5}/C catalyst at 180 °C. Notably, DFT calculations and qNMR studies confirmed that the molecular H₂O not only supplied the hydrogen but also acted as an indispensable promoter to enhance the catalytic performance of Pd_{0.5}Cu_{0.5}/C for methanol activation. Furthermore, the *operando* ATR-FTIR revealed that the mechanism of methanol oxidation to generate hydrogen is CH₃OH → HCHO → HCOOH, and the HCO₃⁻ is reduced into formate with the *in situ* formed hydrogen. The present study provided a potential way towards simple and green one-step CO₂ capture and utilization, which is of great interest in the practical application of CO₂ conversion.

Conflicts of interest

There are no conflicts to declare.

Acknowledgements

The authors thank the financial support of the National Key R&D Program of China (2018YFC0309800 and 2017YFC0506004), the National Natural Science Foundation of China (No. 21978170), the National Science Foundation of Shanghai (No. 19ZR1424800), the National Postdoctoral Program for Innovative Talent (No. BX20200208), the Oceanic Interdisciplinary Program of Shanghai Jiao Tong University (No. SL2020MS022), Start-up Fund for Youngman Research at SJTU, and the Centre of Hydrogen Science, Shanghai Jiao Tong University, China.

Notes and references

1. A. Barthel, Y. Saih, M. Gimenez, J. D. A. Pelletier, F. E. Kühn, V. D'Elia and J. M. Basset, *Green Chem.*, 2016, **18**, 3116-3123.
2. D. W. Keith, G. Holmes, D. S. Angelo and K. Heidel, *Joule*, 2018, **2**, 1573-1594.
3. E. S. Sanz-Perez, C. R. Murdock, S. A. Didas and C. W. Jones, *Chem. Rev.*, 2016, **116**, 11840-11876.
4. S. Das, J. Pérez-Ramírez, J. Gong, N. Dewangan, K. Hidajat, B. C. Gates and S. Kawi, *Chem. Soc. Rev.*, 2020, **49**, 2937-3004.
5. M. Ding, R. W. Flaig, H.-L. Jiang and O. M. Yaghi, *Chem. Soc. Rev.*, 2019, **48**, 2783-2828.
6. H. Zhong, K. Fujii and Y. Nakano, *J. Electrochem. Soc.*, 2017, **164**, F923-F927.
7. S. H. Kim, K. H. Kim and S. H. Hong, *Angew. Chem. Int. Ed.*, 2014, **53**, 771-774.
8. H. Zhong, K. Fujii, Y. Nakano and F. Jin, *J. Phys. Chem. C*, 2015, **119**, 55-61.
9. H. Zhong, M. Iguchi, M. Chatterjee, Y. Himeda, Q. Xu and H. Kawanami, *Adv. Sustain. Syst.*, 2018, **2**, 1700161.
10. H. Zhong, M. Iguchi, M. Chatterjee, T. Ishizaka, M. Kitta, Q. Xu and H. Kawanami, *ACS Catal.*, 2018, **8**, 5355-5362.
11. R. Navarro, M. Sanchez-Sanchez, M. Alvarez-Galvan, F. Del Valle and J. Fierro, *Energy Environ. Sci.*, 2009, **2**, 35-54.
12. S. Choi, T. C. Davenport and S. M. Haile, *Energy Environ. Sci.*, 2019, **12**, 206-215.
13. G. W. Huber, J. Shabaker and J. Dumesic, *Science*, 2003, **300**, 2075-2077.
14. D. M. Alonso, J. Q. Bond and J. A. Dumesic, *Green Chem.*, 2010, **12**, 1493-1513.
15. F. Jin, Y. Gao, Y. Jin, Y. Zhang, J. Cao, Z. Wei and R. L. Smith Jr, *Energy Environ. Sci.*, 2011, **4**, 881.
16. J. Duo, F. Jin, Y. Wang, H. Zhong, L. Lyu, G. Yao and Z. Huo, *Chem Comm*, 2016, **52**, 3316-3319.
17. H. Zhong, L. Wang, Y. Yang, R. He, Z. Jing and F. Jin, *ACS Appl. Mater. Interfaces*, 2019, **11**, 42149-42155.
18. H. Zhong, G. Yao, X. Cui, P. Yan, X. Wang and F. Jin, *Chem. Eng. J.*, 2019, **357**, 421-427.
19. M. Wang, M. Liu, J. Lu and F. Wang, *Nat. Commun.*, 2020, **11**, 1-9.
20. M. Liu, Y. Wang, X. Kong, R. T. Rashid, S. Chu, C.-C. Li, Z. Hearne, H. Guo, Z. Mi and C. J. Li, *Chem*, 2019.
21. Z. Luo, Y. Ouyang, H. Zhang, M. Xiao, J. Ge, Z. Jiang, J. Wang, D. Tang, X. Cao and C. Liu, *Nat. Commun.*, 2018, **9**, 1-8.
22. N. J. Johnson, B. Lam, B. P. MacLeod, R. S. Sherbo, M. Moreno-Gonzalez, D. K. Fork and C. P. Berlinguette, *Nat. Mater.*, 2019, **18**, 454-458.
23. J. D. A. Pelletier and J. Basset, *Acc. Chem. Res.*, 2016, **49**, 664-677.
24. M. K. Samantaray, V. Delia, E. Pump, L. Falivene, M. Harb, S. O. Chikh, L. Cavallo and J. Basset, *Chem. Rev.*, 2020, **120**, 734-813.
25. S. Kattel, P. Liu and J. G. Chen, *J. Am. Chem. Soc.*, 2017, **139**, 9739-9754.
26. T. Schedel-Niedrig, M. Hävecker, A. Knop-Gericke and R. Schlögl, *Phys. Chem. Chem. Phys.*, 2000, **2**, 3473-3481.
27. H. Bluhm, M. Hävecker, A. Knop-Gericke, E. Kleimenov, R. Schlögl, D. Teschner, V. I. Bukhtiyarov, D. F. Ogletree and M. Salmeron, *J. Phys. Chem. B*, 2004, **108**, 14340-14347.
28. H. Duan, J. C. Liu, M. Xu, Y. Zhao, X. L. Ma, J. Dong, X. Zheng, J. Zheng, C. S. Allen, M. Danaie, Y. K. Peng, T. Issariyakul, D. Chen, A. I. Kirkland, J. C. Buffet, J. Li, S. C. E. Tsang and D. O'Hare, *Nat. Catal.*, 2019.
29. F. Jin and H. Enomoto, *Energy Environ. Sci.*, 2011, **4**, 382-397.
30. Y. Zhang, Z. Shen, X. Zhou, M. Zhang and F. Jin, *Green Chem.*, 2012, **14**, 3285-3288.
31. L. Lu, H. Zhong, T. Wang, J. Wu, F. Jin and T. Yoshioka, *Green Chem.*, 2020, **22**, 352-358.
32. F. M. Jin, A. Kishita, T. Moriya and H. Enomoto, *J. Supercrit. Fluids*, 2001, **19**, 251-262.
33. N. Yang, Z. Zhang, B. Chen, Y. Huang, J. Chen, Z. Lai, Y. Chen, M. Sindoro, A. L. Wang and H. Cheng, *Adv. Mater.*, 2017, **29**, 1700769.
34. X. Huang, S. Tang, X. Mu, Y. Dai, G. Chen, Z. Zhou, F. Ruan, Z. Yang and N. Zheng, *Nat. Nanotechnol.*, 2011, **6**, 28.
35. W.-C. Cheong, C. Liu, M. Jiang, H. Duan, D. Wang, C. Chen and Y. Li, *Nano Res.*, 2016, **9**, 2244-2250.
36. Z. Guo, X. Kang, X. Zheng, J. Huang and S. Chen, *J. Catal.*, 2019, **374**, 101-109.
37. F. Pang, Z. Wang, K. Zhang, J. He, W. Zhang, C. Guo and Y. Ding, *Nano Energy*, 2019, **58**, 834-841.
38. J. Fan, S. Yu, K. Qi, C. Liu, L. Zhang, H. Zhang, X. Cui and W. Zheng, *J. Mater. Chem. A*, 2018, **6**, 8531-8536.
39. G. W. Huber, J. W. Shabaker, S. T. Evans and J. A. Dumesic, *Appl. Catal. B*, 2006, **62**, 226-235.
40. J. Greeley and M. Mavrikakis, *Nat. Mater.*, 2004, **3**, 810-815.
41. X. Yu, X. Tian and S. Wang, *Surf. Sci.*, 2014, **628**, 141-147.
42. G. C. Wang, Y. H. Zhou and J. Nakamura, *J. Chem Phys.*, 2005, **122**, 044707.
43. H. Ma, G. Wang, Y. Morikawa and J. Nakamura, *Sci. China. Ser. B*, 2009, **52**, 1427-1433.
44. Y. Yang, H. Zhong, R. He, X. Wang, J. Cheng, G. Yao and F. Jin, *Green Chem.*, 2019, **21**, 1247-1252.
45. A. Rodes, E. Pastor and T. Iwasita, *J. Electroanal. Chem.*, 1994, **376**, 109-118.
46. L. F. Liao, C. F. Lien, D. L. Shieh, M. T. Chen and J. L. Lin, *J. Phys. Chem. B*, 2002, **106**, 11240-11245.
47. N. A. Anan, S. M. Hassan, E. M. Saad, I. S. Butler and S. I. Mostafa, *Carbohydr. Res.*, 2011, **346**, 775-793.
48. J. De Souza, S. Queiroz, K. Bergamaski, E. R. Gonzalez and F. C. Nart, *J. Phys. Chem. B*, 2002, **106**, 9825-9830.
49. T. Wang, D. Ren, Z. Huo, Z. Song, F. Jin, M. Chen and L. Chen, *Green Chem.*, 2017, **19**, 716-721.
50. J. Su, M. Lu and H. Lin, *Green Chem.*, 2015, **17**, 2769-2773.